RAPID COMMUNICATIONS

PHYSICAL REVIEW A VOLUME 43, NUMBER 6 15 MARCH 1991

Space- and time-resolved $K\alpha$ absorption spectroscopy of a laser-produced plasma

J. P. Geindre, C. Chenais-Popovics, P. Audebert, C. A. Back, and J. C. Gauthier
Laboratoire de Physique des Milieux Ionisés and Laboratoire d'Utilisation des Lasers Intenses, Ecole Polytechnique, 91120 Palaiseau, France

H. Pépin and M. Chaker
Institut National de la Recherche Scientifique Energie, Case Postale 1020, Varennes, Québec, Canada
(Received 2 January 1991)

We have studied the space and time evolution of the dense part of a laser-produced plasma obtained on a target composed of a chlorinated plastic foil covered with a samarium layer. With point-projection $K\alpha$ absorption spectroscopy we measured the optical depth and the electronic temperature of the radiatively heated plasma as a function of time and space. Radiative hydrocode simulations describe correctly the experimental results. The plasma zone radiatively heated at 50–80 eV by the laser-irradiated samarium soft x rays expands just after the laser maximum when the laser-induced pressure has decreased. The obtained dense plasma exhibits shallow density and temperature gradients and could be used for dense-plasma studies.

In the past years, much effort has been directed into the understanding of the role of radiative transfer in laser-plasma interactions. Soft x rays play a dominant role in the plasmas produced by elements of high atomic number. They heat the target more deeply than the electronic conduction, establishing an extended "reemission zone" of intermediate temperatures (around 100 eV).[1] Experiments based on inner-shell x-ray absorption spectroscopy have proven to be an excellent diagnostic of these high-density and low-temperature plasmas.[2–6] X rays emitted by a laser-irradiated high-Z layer create a radiative heat wave in the lower-Z substrate of a multilayered target. The diagnostic relies on the ability of this substrate, or an embedded layer, to exhibit a $K\alpha$ or $L\alpha,\beta$ absorption spectrum when illuminated by a backlighter source.

Until now, experiments have mostly been done with a single laser beam focused on a multilayered target. Using a separated x-ray backlighter enables temporal and spatial investigation of the plasma. This last technique has already been successfully used on H-like and He-like Rydberg series lines.[7] It is an excellent potential diagnostic of ionization, temperature, and density in x-ray laser plasmas following a recombination scheme or a neonlike collisional excitation scheme.[6] Coupled with inner-shell $K\alpha$ line absorption, point-projection backlighting leads to a deeper knowledge of the radiatively heated plasma, as will be shown in this paper.

In the present experiment, we study the plasma created on a target composed of a chlorinated plastic foil covered with a samarium layer directly irradiated by the laser. The soft x-ray emission of samarium heats the chlorinated plastic at temperatures adequate to produce F-like to B-like chlorine ions. We measure the $K\alpha$ absorption lines of these ion species as well as the continuum absorption of the samarium layer as a function of space by point projection spectroscopy. Time history is obtained by changing the delay of the laser produced x-ray backlighter. The behavior of the plasma is well understood by comparing the time and space dependence of the experimental spectra with radiative hydrocode simulations post processed by a detailed atomic physics program package.

The experiments were performed with two beams of the Nd-glass laser of the Laboratoire d'Utilisation des Lasers Intenses (LULI). First, a frequency-doubled ($\lambda=0.53$ μm) laser beam (called hereafter "main beam") was incident at 25° from the normal to the target and focused into a 180-μm-diameter spot on a 0.4-μm Sm layer deposited onto 12.5 μm of $(C_2H_2Cl_2)_n$. This foil was rolled onto a glass stalk in order to avoid target edge shadowing and to permit axial resolution along the target normal. For a few shots, we have mounted the Sm/(CHCl) foil free-standing perpendicular to the spectrograph axis giving access to radial resolution along the target surface. Laser intensity was 1.5×10^{14} W/cm^2. The resulting plasma (called later on "the plasma") is the object of the present study.

A second beam was frequency quadrupled ($\lambda=0.26$ μm) and tightly focused onto the end of a 100-μm-diameter lead wire in order to provide the backlighter x-ray source (abbreviated hereafter BL). Energy and intensity were 20 J and 10^{15} W/cm^2. Focal spots positions were monitored by an optical microscope coupled with charge-coupled device (CCD) imaging. Pulse duration was 500 ps for both beams. The delay between the backlighter and the main beam was 0–1.4 ns and was measured with a visible streak camera. The BL quality was monitored by a pinhole camera set at 45° above the backlighter laser axis. Several filtered x-ray diodes[3] around the main target normal measured the (0.1–4)-keV range samarium x-ray spectrum. The main diagnostic was a time integrating pentaerythritol (PET) crystal spectrograph working in the 2.5–3-keV range to record the $K\alpha$ lines of chlorine. A 700-μm-diameter tungsten wire set in front of the spectrograph provided a knife-edge penumbral image of the plasma and BL emission.[8]

Figure 1 shows a typical spectrum obtained 940 ps after the main laser-pulse maximum. The target, the BL, the knife edge, and the spectrograph arrangement determines

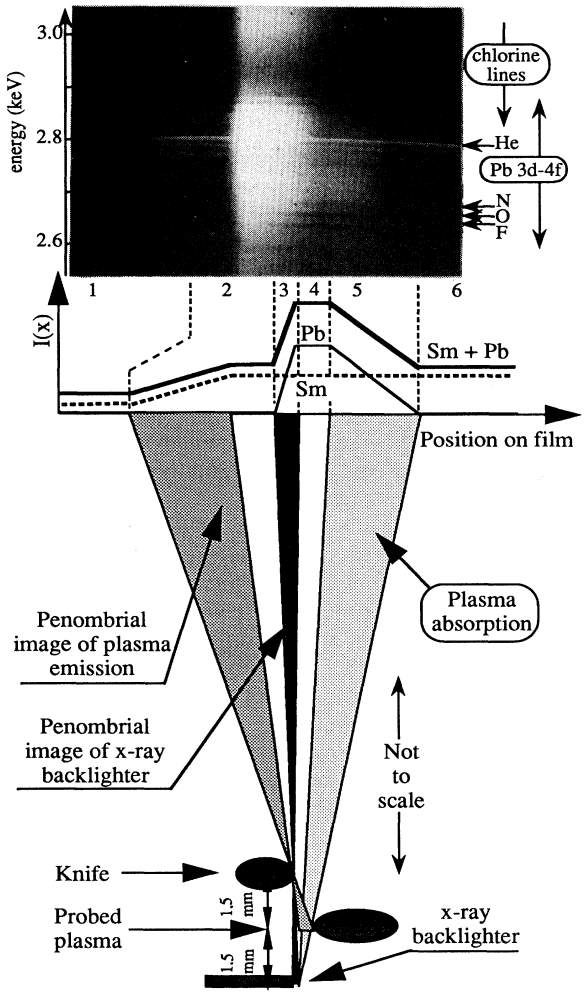

FIG. 1. Schematic experimental arrangement showing the main target, the backlighter and the knife-edge. The crystal of the spectrometer is not represented for clarity. A typical spectrum is shown on the photograph. $K\alpha$ lines of F-, O-, and N-like chlorine ions appear on the $3d$-$4f$ Pb backlighter emission. Time integrated He-like $1s^2$-$1s2p$ line is used for photon energy calibration.

different zones of interest on the film, as the following: (i) film background in zone 1; (ii) penumbral image of plasma emission in zone 2; target surface is the transition between zone 1 and 2; derivative of the digitized intensity in this zone gives the spatial dependence of plasma emission; (iii) penumbral image of BL added to plasma emission; the derivative of the digitized intensity in zone 3 gives the BL size, i.e., the spatial resolution of absorption measurements; (iv) addition of space integrated plasma and BL emissions; (v) absorption of the plasma; the image of the main target surface is at the limit of zones 5 and 6; (vi) space integrated emission of the plasma. The unattenuated BL emission is deduced from intensities in zone 4 and 6. A magnification of 80 is achieved on film.

The $3d$-$4f$ transition array of Pb emission was used for the backlighter. Its apparent size seen from the film is 8 μm as measured from zone 3 on film. During the 500-ps BL duration, samarium exhibits a continuous absorption. The absorption of chlorine consists of the $1s$-$2p$ lines originating from Cl^{8+}-Cl^{11+} ions (F- to C-like), and near the chlorine K edge, the $1s$-$3p$ absorption lines originating from Cl^{6+}-Cl^{11+} ions (Al- to C-like). The chlorine and samarium emission is time integrated. Samarium has been chosen for its low emission in the chlorine $K\alpha$ lines range. Chlorine emits the He-like $1s^2$-$1s2p$ line that we have used for calibration of the spectral dispersion.

Analysis of the experimental data consisted in tracing the spectra in the 4–5-Å range for different positions on film at different times (460, 710, 940, and 1400 ps after the peak of the main laser pulse). We have concentrated here on the spatial and temporal behavior of the samarium continuum and $1s$-$2p$ chlorine lines. The optical depth is deduced from the spectra by the usual absorption formula $\tau = -\ln(I/I_0)$ where the BL intensity I_0 is measured in the outer part of the plasma where absorption is negligible. We have also deduced the electronic temperature from the chlorine $K\alpha$ lines ratios as a function of space and time.

Numerical simulations were performed with the one-dimensional radiative hydrocode XRAD.[9] Target was a 0.4-μm Sm layer deposited onto 60 μm of $(C_2H_2Cl_2)_n$ plastic and incident laser intensity was 2×10^{14} W/cm^2. Also, we have run simulations with 0.3-μm Sm and 1×10^{14} W/cm^2 when specified. Thermal conductivity was described by Spitzer with a 0.05 factor limited heat flux. Absorption coefficients and ionization balance were deduced from a nonlocal-thermal-equilibrium (non-LTE) average-atom model. In order to compare directly the experimental optical depth with code predictions, we have introduced space and time integration of BL emission assuming experimental plasma and backlighter conditions.

We have first measured the front x-ray emissivity of the samarium layer and compared it to the simulations. X-ray diodes measurements and simulations showed two peaks of emission in the range 200–400 eV and 1–2 keV corresponding, respectively, to the N- and M-band. The total integrated x-ray energy was 5×10^{15}–1×10^{16} keV/sr representing 26% ± 6% conversion ratio. XRAD calculations gave 29.7% total conversion. This was distributed as 18% (18.2% in the calculation) in the 0–1-keV range and 8% (11% in the calculation) in the 1–4-keV range. In order to check that this samarium x-ray emission is responsible of the heating of chlorine in the target, we shot a few targets of pure chlorinated plastic. No $K\alpha$ absorption lines were visible; in this case the dynamics of the plasma is governed by thermal conductivity, and the 100-eV region in which chlorine F- to Li-like ions appear is limited to a region of the thermal front too small to be diagnosed.

Simulation results in Fig. 2 show the plasma evolution by the trajectories of the cells. The laser-ablated samarium expands rapidly towards vacuum (zone 1). The samarium not ablated by the laser is easily identified by the region where trajectories are densely packed (zone 2). At the beginning of the pulse, the samarium layer starts to be ablated by radiative heating. At the pulse maximum, laser-ablation pressure confines the samarium, and the radiative wave reaches the chlorinated plastic which starts to blow away (zone 3). After the laser pulse, the laser-induced ablation pressure decreases and the samarium

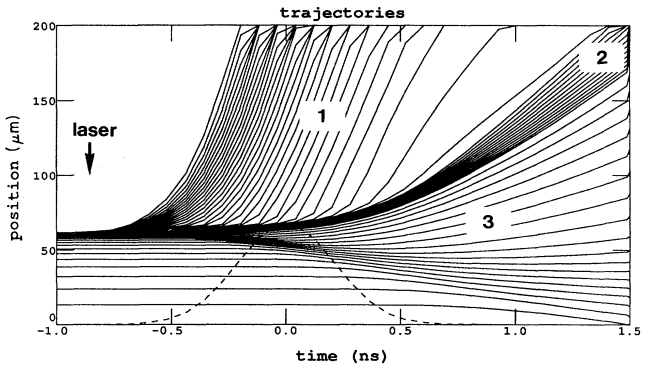

FIG. 2. Trajectories of the cells calculated with XRAD code for 2×10^{14} W/cm^2 laser intensity incident onto 0.4-μm Sm. Zone 1: expanding ablated matter; zone 2: nonablated samarium; zone 3: radiatively heated chlorinated plastic.

layer expands towards vacuum. It is in this late stage that the radiatively heated samarium and chlorinated plastic (zones 2 and 3) have sufficient extension for axial measurements of the optical depth. Zones 2 and 3 correspond to the radiatively heated temperature plateau of 50–80 eV appearing after the laser pulse.

Figure 3 shows plots of the experimental and averaged optical depth given by the code as a function of distance along the target normal for different x-ray probing times. The spectral range covers samarium and chlorine absorption from the chlorine K edge to $K\alpha$ lines (2.62–2.84 keV). At later times, the optical depth exhibits a plateau and bends with a smooth fall-off. The position and velocity of the bend are physically meaningful. The position of the bend corresponds exactly to the outer edge of the absorbing plasma at the beginning of the BL pulse duration. Thus, the fall-off is due to the displacement of the absorbing region during probing time. This is shown in the simulation by the displacement of the sharp variation of transmitted intensity located at the edge of the absorbing plasma.

Comparison of Fig. 3(a)–3(d) show the spread of the dense absorbing region after the laser-pulse maximum. Measurements taken at laser-pulse maximum showed no expansion. Experimental and calculated data are very close in positions as well as absolute values. Figure 2 explains well the experimental results that have measured the radiatively heated region after the laser pulse, when laser-induced pressure has decreased. The bump situated around 100 μm in Fig. 3(d) corresponds to Sm absorption as identified in zone 2 in Fig. 2. The only discrepancy between code and experiments is that the outer fall of the optical depth propagates slightly more rapidly in the code.

We have compared in Fig. 4 the experimental and calculated position of the bend of Fig. 3 plots as a function of time for different code conditions. Although experimental and calculated trajectories of the bend cross each other, simulations give a good overall agreement. The expansion velocity is lower in the experiment than in the calculation, but the initial position of the bend is situated further out along the target normal. This discrepancy is not explained by changes in laser or target conditions as shown in Fig. 4. It could be linked to two-dimensional behavior of the plasma in the following way: at early times, the edges of the focal spot can be pushed towards vacuum and absorb further out than the on-axis plasma; at later times, expansion is partially spherical inducing less expansion along the target normal.

We have analyzed the $K\alpha$ absorption lines to get a measurement of the electronic temperature gradients of the chlorinated plastic. In the shots giving radial resolution, we have seen an ionization state constant in the focal spot and decreasing at the edges. This is the sign of a radially

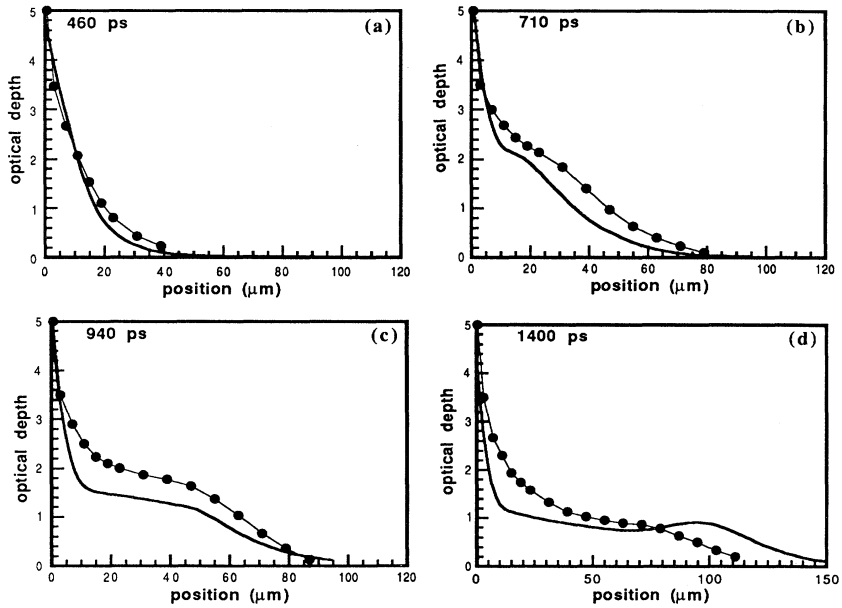

FIG. 3. Comparison of experimental (dots) and calculated (solid line) optical depth in the range 2.6–2.8 keV as a function of distance along target normal at different times (460, 710, 940, and 1400 ps after laser maximum).

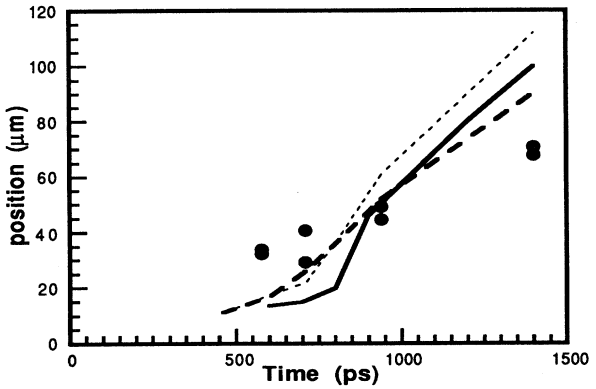

FIG. 4. Position of the bend of optical depth (of Fig. 3) as a function of time. Origin of time is the peak of the laser pulse. Experimental results are compared to simulations for different conditions: solid line: 2×10^{14} W/cm^3, 0.4-μm Sm; dashed line: 1×10^{14} W/cm^3, 0.4-μm Sm; dotted line: 1×10^{14} W/cm^3, 0.3-μm Sm.

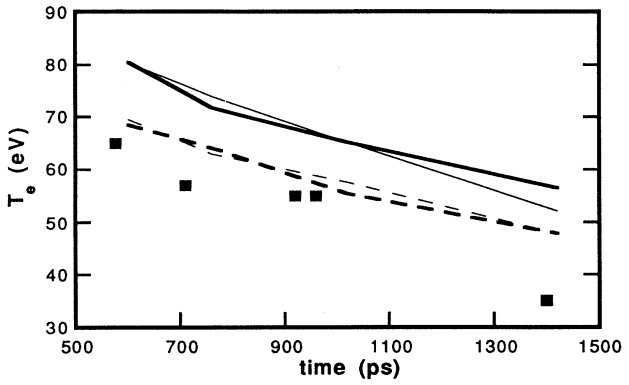

FIG. 5. Electronic temperature of the radiatively heated zone as a function of time. Origin of time is the peak of the main pulse. Experiment: dots; solid line: 2×10^{14} W/cm^3, 0.4-μm Sm; thin-solid line: 2×10^{14} W/cm^3, 0.3-μm Sm; dashed line: 1×10^{14} W/cm^3, 0.4-μm Sm; thin-dashed line: 1×10^{14} W/cm^3, 0.3-μm Sm.

homogeneous temperature surrounded by gradients. In the shots with axial resolution, $K\alpha$ absorption line ratios remain constant along the target normal as seen in the photo in Fig. 1. This leads to the important conclusion that temperature is constant in the CHCl plasma along the target normal. Simulations agree with this last observation as the chlorine $K\alpha$ lines appear in the radiatively heated temperature plateau. Also, we have measured the time variation of the electronic temperature in the chlorinated plastic by comparing at different times the experimental $K\alpha$ absorption lines to calculations done with a LTE modeling of the detailed spectrum.[10] A 0.1-g/cm^3 density has been taken from the simulations. Figure 5 shows the comparison between the experimental and calculated electronic temperature as a function of time for different code conditions. The agreement is very good for the time decrease of temperature. Experimental temperature is about 10% lower than in the code. This could be expected as $K\alpha$ absorption lines are space-integrated along the target surface including the cold plasma situated around the focal spot.

In summary, we have measured the spatial and temporal behavior of a radiatively heated Sm/CHCl plasma. We have verified the time evolution of its optical depth and temperature as predicted by XRAD simulations. We have shown that the plasma expansion due to radiative heating occurs after the laser pulse when laser-induced ablation pressure decreases. This type of plasma could be a good alternative to classical exploded foils in order to prepare a large homogeneous plasma for the study of radiative transfer,[11] laser interaction, or x-ray lasers.

We thank the staff of the LULI for technical support and the Paris-Sud University teams in Centre de Densitométrie et de Synthèse d'Images for film densitometry, in Centre Inter-Régional de Calcul Electronique for numerical assistance, and in Institut de Physique Nucléaire for target fabrication.

[1]K. Eidmann, R. F. Schmalz, and R. Sigel, Phys. Fluids B **2**, 208 (1990), and references therein.

[2]A. Hauer, R. W. Cowan, B. Yaakobi, O. Barnouin, and R. Epstein, Phys. Rev. A **34**, 411 (1986).

[3]C. Chenais-Popovics, C. Fievet, J. P. Geindre, J. C. Gauthier, J. F. Wyart, and E. Luc-Koenig, Phys. Rev. A **40**, 3194 (1989).

[4]C. Chenais-Popovics, C. Fievet, J. C. Gauthier, J. P. Geindre, M. Klapisch, J. P. Lebreton, M. Louis-Jacquet, D. Naccache, and J. P. Perrine, Phys. Rev. Lett. **65**, 1435 (1990).

[5]J. C. Gauthier, J. P. Geindre, C. Chenais-Popovics, M. Louis-Jacquet, J. Bruneau, D. Desenne, D. Naccache, C. Bauche-Arnoult, and J. Bauche, in *Proceedings of the International Workshop on Radiation Transfer Properties of Hot Dense Matter 1990* (World Scientific, Singapore, in press).

[6]C. L. S. Lewis, J. E. Balmer, J. D. Kilkenny, A. Bar-Shalom, S. J. Rose, W. Goldstein, A. Osterheld, S. Davidson, and R. W. Lee, in *Proceedings of the International Workshop on Radiation Transfer Properties of Hot Dense Matter* (Ref. 5).

[7]D. M. O'Neill, D. Neely, C. L. S. Lewis, S. J. Davidson, S. J. Rose, and R. W. Lee, in Proceedings of the Second International Colloquium on X-Ray Lasers Proceedings, York, United Kingdom, 1990 (unpublished).

[8]P. Alaterre, C. Popovics, J. P. Geindre, and J. C. Gauthier, Optics Commun. **49**, 140 (1984).

[9]J. C. Gauthier and J. P. Geindre, Rapport Annuel GRECO ILM, Report No. 176, 1988 (unpublished), available upon request from the authors.

[10]C. Chenais-Popovics, C. Fievet, J. P. Geindre, I. Matsushima, and J. C. Gauthier, Phys. Rev. A **42**, 4788 (1990); E. Luc-Koenig, M. Klapisch, and A. Bar-Shalom, computer code RELAC.

[11]C. A. Back, C. Chenais-Popovics, J. C. Gauthier, R. W. Lee, J. I. Castor, J. Edwards, L. Gizzi, and O. Willi, in *Proceedings of the International Workshop on Radiation Transfer Properties of Hot Dense Matter* (Ref. 5).

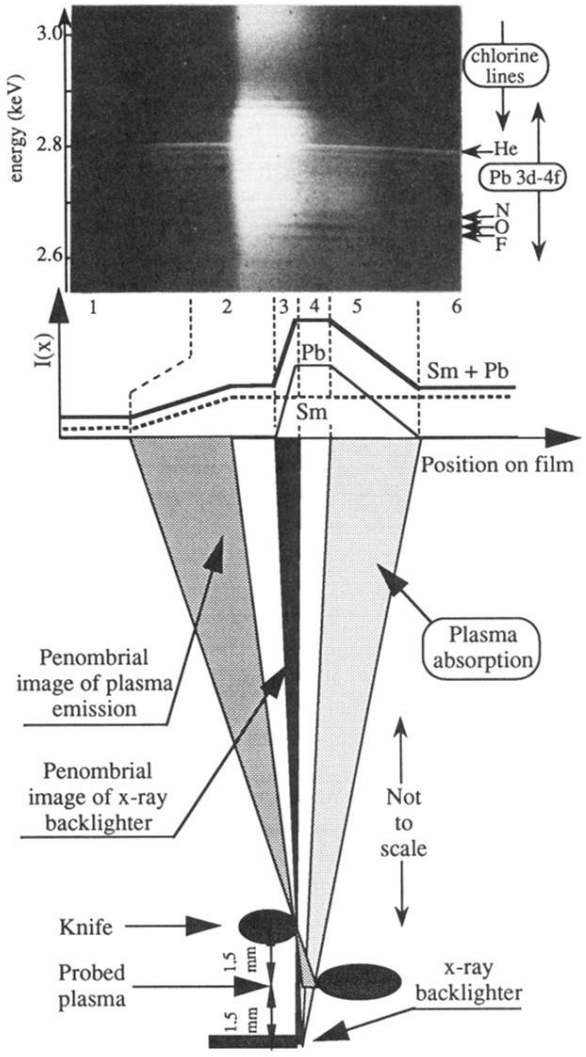

FIG. 1. Schematic experimental arrangement showing the main target, the backlighter and the knife-edge. The crystal of the spectrometer is not represented for clarity. A typical spectrum is shown on the photograph. $K\alpha$ lines of F-, O-, and N-like chlorine ions appear on the $3d$-$4f$ Pb backlighter emission. Time integrated He-like $1s^2$-$1s2p$ line is used for photon energy calibration.